Wideband and High-Efficiency Circularly Polarized Unit-Cell for X and Ka-Band Transmitarrays

Alessandro de Oliveira Cabral Junior, Hamza Kaouach, André Barka

Received 12 April 2024; revised 30 May 2024; accepted 2 June 2024. Date of publication 10 June 2024; date of current version 6 August 2024.

Digital Object Identifier 10.1109/OJAP.2024.3409746

Wideband and High-Efficiency Circularly Polarized Unit-Cell for X and Ka-Band Transmitarrays

ALESSANDRO DE OLIVEIRA CABRAL JUNIOR [1,2], HAMZA KAOUACH [2], AND ANDRÉ BARKA [1]

[1]ONERA/DEMR, Université de Toulouse, 31055 Toulouse, France
[2]LAPLACE Laboratory, Université de Toulouse INP-ENSEEIHT, 31029 Toulouse, France

CORRESPONDING AUTHOR: A. BARKA (e-mail: andre.barka@onera.fr)

This work was supported in part by the Grand Équipement National De Calcul Intensif (GENCI) from which the full-wave simulation results have been obtained using HPC resources under Grant c2014109083.

ABSTRACT This paper presents a novel approach for linear to circular polarization (LP-CP) conversion in transmitarray antennas. The proposed conversion mechanism differs significantly from previous published realizations. The concept utilizes a transmission line modeling-based excitation technique, in which a centralized via excitation is split into two striplines carefully designed to balance excitations and guarantee a phase quadrature. The striplines are embedded at the center of the patch antenna allowing a compact footprint and a simple design structure. The applied true-time delay (TTD) technique assures the radiation of a wideband and low axial ratio circularly polarized (CP) field. To optimize bandwidth and transmission efficiency, a stacked patch configuration is also employed, allowing for simultaneous high polarization conversion and transmission efficiency. The unit-cell design methodology is detailed, and two transmitarray designs are realized in both X and Ka bands. Experimental results from a fabricated X-band 20×20 cell array prototype demonstrate a peak aperture efficiency of 30%, accompanied by a simultaneous 16% -1 dB gain and 1 dB axial ratio bandwidths. Furthermore, the measured wideband and highly efficient Ka-band transmitarray with a 70×70 cell array confirmed a remarkable gain of 39.8 dB and 55% aperture efficiency at 29 GHz, surpassing previous LP-CP transmitarray antennas, while maintaining axial ratio values below 1 dB in a bandwidth larger than 26%.

INDEX TERMS Transmitarray, phased array, unit-cell, stacked patch, polarization conversion, circular polarization, axial ratio, wideband, X-band, Ka-band.

I. INTRODUCTION

THE CURRENT trend in modern telecommunications systems is the migration towards higher frequency bands. The use of millimeter wave frequencies, including the Ka, E, D, and W-bands, allows future applications such as 5G mmWave for front-haul and backhaul links [1], [2], Satellite Communications (SatCom) in LEO [3] and GEO orbits, radars [4] and imaging applications [5]. However, this shift presents its own set of technological challenges for the design and fabrication of advanced antenna systems, that should answer to the requirements of these new applications. To compensate for the higher propagation losses, the antennas require a higher gain. Additionally, precise beam-forming and beam-steering are necessary to reduce interference among users and increase signal strength.

Transmitarray antennas (TA) are commonly referred to as flat or discrete lenses due to their planar geometry, distinguishing them from traditional microwave lenses. The TA aperture consists of multiple discrete unit-cells (UCs) that receive illumination from an incoming spherical wavefront. These UCs then transmit and phase-shift the incoming field to generate a controlled outgoing wavefront. Typically, horn antennas or planar arrays serve as source feeds, producing one or more high-gain pencil-shaped beams with controlled apodization. Apodization refers to the gradual attenuation of excitation towards the aperture's edges, allowing antenna systems to exhibit improved performance by minimizing side lobe levels (SLLs) and customizing the beam shape. As a result of ongoing research on advanced UC principles, TA antennas have found various applications beyond their

standard configuration. This research has yielded diverse structures that offer intriguing features to these antennas.

Over the past decade, TA antennas have gained significant attention as an alternative to traditional approaches such as phased arrays, reflector antennas, and antenna lenses. This is due to the fact that TAs offer smaller losses and lower costs compared to phased arrays, primarily because they lack a beamforming network (BFN). Furthermore, they do not suffer from feed blockage and the fabrication complexity is smaller when compared to microwave lenses.

This work focuses on developing UCs for polarization conversion, specifically for converting a linearly polarized (LP) incoming field to an outgoing circularly polarized (CP) field in mmWave SatCom and 5G backhauling applications. Circular polarization offers advantages in SatCom applications by reducing polarization mismatch losses caused by antenna misalignment, minimizing multi-path reflection interference, and enhancing resistance to atmospheric conditions. The use of LP feeds simplifies the design of the focal source due to cost-effectiveness, design simplicity, and manufacturing feasibility. Furthermore, future 5G mmWave backhauling applications demand wider bandwidths to meet the growing data consumption requirements. To ensure reliable and high-speed connections for mobile users in 5G heterogeneous networks [6], mmWave antennas with relative -1 dB gain bandwidths exceeding 15% and aperture efficiency exceeding 40% have been demonstrated using a single linearly polarized transmitarray [1]. In addition, in order to respect radiation masks imposed by international organisms such as [7], axial ratio values under 0.8 dB are sought. These performance indicators will serve as design goals for this work, serving as a comparative standard among different solutions.

Previous works have explored the use of sequentially rotated LP UCs to generate a CP field. For example, in [8], a LP UC based on circular patches loaded with dual C-shaped slots is utilized. However, this approach suffers from a major drawback of 3 dB losses due to the sequential rotation mechanism with LP UCs. Although it achieves a wide 3 dB axial ratio bandwidth, it exhibits limited aperture efficiency of only 24%. Thus, to overcome the 3 dB conversion loss associated with LP UCs, CP UCs must be employed.

Several CP structures have been proposed in the literature as the transmit (Tx) antenna of the UCs. These include CP magnetoelectric (ME) dipoles [9], circular patches with asymmetrical slots [10], [11], and truncated corner patches [12], [13]. Among these realizations, the CP ME dipole achieves the largest 3 dB axial ratio bandwidth of over 33%. However, these CP UCs suffer from high axial ratio values and present narrowband CP operation. Therefore, the use of sequential rotation is still applied to achieve wideband axial ratio behavior.

An alternative approach to polarization converter and phase shifting UCs is the use of external polarizers. Two recent works, [14] and [15], propose similar designs based on multilayer frequency selective surfaces (MFSS) for dual-band, dual-linear-to-circular polarization converters. However, one inherent limitation of MFSS is its narrowband nature, resulting from the use of resonant structures [16]. As a result, the 3 dB axial ratio bandwidth limited to 7%. Moreover, the use of an external polarizer requires the use of two apertures to incorporate beam-forming and steering functionalities.

Recently, a reconfigurable LP-CP concept has been proposed by [17]. This concept utilizes a 2-bit reconfigurable LP-LP UC that incorporates PIN diodes to switch between four phase states. In addition, a reconfigurable polarizer featuring an asymmetrical U-slotted patch antenna, which can switch between CP modes by controlling two PIN diodes, is used. However, this approach faces several challenges. Firstly, the use of six PIN diodes leads to increased insertion losses, with a minimum loss of 2 dB. Secondly, the axial ratio bandwidth of the polarizer stage is narrow, reaching a maximum of 15% with a -3 dB transmission criteria. Lastly, the overall design complexity is increased due to the requirement of three bias lines per UC and the coupling between two apertures.

The development of LP-CP UCs with wide axial ratio bandwidth, high efficiency, and low losses is critical for the design of high-performance, cost-effective CP transmitarrays with LP feeds. Previous studies have proposed the use of external polarizers, sequential rotation and narrow band CP antennas on the UC. However, these approaches have limitations such as narrow bandwidths and low aperture efficiencies.

In our work, we present a novel design procedure and optimization of a polarization conversion and phase shifting UC that does not require external polarizers. To the best of the authors' knowledge, the proposed UC utilizes a novel CP conversion mechanism that has never been previously published.

The concept includes a CP patch antenna based on the transmission line theory, coupled with a stacked annular ring patch to achieve high radiation efficiency and wide transmission and axial ratio bandwidths. In comparison to previous circular polarization (CP) UCs, such as those discussed in [9], [11], and [13], this study introduces novel contributions. Firstly, the circular polarization conversion mechanism employed in this work differs significantly, as the generation of CP fields is accomplished by employing a dual excitation technique with carefully designed transmission lines to achieve CP. Secondly, the UC itself demonstrates a wide axial ratio bandwidth exceeding 16%, which surpasses all previous realizations. This wide bandwidth is accompanied by high transmission efficiency, with insertion losses (IL) inferior to 0.3 dB, and a -1 dB transmission bandwidth exceeding 13%. Lastly, the advantage of this approach is that it eliminates the need for sequential rotation mechanisms, or the use of external polarizers. The novel proposed approach employs a single aperture that integrates both beam-forming and polarization conversion capabilities.

This enables a simpler, more efficient, and cost-effective design.

The proposed UC is analyzed by Floquet modes excitation using CST Microwave Studio, the complete TA antenna is optimized using a semi-analytical tool [18] and an HPC full-wave solver [19], [20]. The semi-analytical tool enables a meticulous design of the complete antenna through parametric studies, while the HPC full-wave solver enables the fast and precise characterization of the final electrically large apertures.

Two versions of the proposed UC are designed. First as a proof-of-concept, a X-Band UC centered at 10.25 GHz has been realized, it achieves 13% −1 dB transmission and 16% 3 dB axial ratio bandwidths. A 20×20 cells TA using 2-bits of quantization has been designed, fabricated and measured to demonstrate the superior performance of CP UCs in comparison with the previous mentioned works. It achieves 16% −1 dB gain bandwidth, with peak aperture efficiency at 33%. Throughout the whole measured band the axial ratio values are under 1 dB, thus more than 30% 3 dB axial ratio BW is achieved. At the Ka band (30 GHz), the UC concept is further optimized to achieve a simultaneous −1 dB transmission and 3 dB axial ratio bandwidth of more than 18%. In addition, a mmWave TA antenna with a very large aperture of 70×70 cells ($35\lambda_0$ in diameter) has been designed and measured, it achieves a peak aperture efficiency of 55%, which is higher than all the other previous realizations and greatly surpasses the 40% aperture efficiency criteria for mmWave backhauling applications. The higher aperture efficiency and wider axial ratio bandwidth of the proposed UC make it a promising candidate for high-efficiency, wide-band, and low-cost CP transmitarrays. This study provides a significant contribution to the development of LP-CP UCs and can pave the way for the design of more advanced and efficient CP transmitarrays.

The rest of the work is organized as follows. In Section II the initial concept idea, its working mechanism and evolution are presented. Then, the design procedure of the CP UC is detailed and in Section III the TA design and its optimization are demonstrated through simulations and measurements. Finally, conclusions are drawn in Section IV.

II. CIRCULARLY POLARIZED UNIT-CELL CONCEPT AND DESIGN

Our previous work established a transmission line modeling for designing inner feed linearly polarized unit-cells [18]. In this section, this modeling will be further expanded to generate a linear to circular (LP-CP) polarization converter and phase shifting unit-cell. This innovative concept enables the UC to directly convert the incoming LP field into a low axial ratio and wide-band CP field, without requiring a sequential rotation mechanism, which eliminates the 3 dB losses from using sequentially rotated LP unit-cells [8]. Thus, this novel UC will enable the design of a much more efficient TA antenna, with lower and more stable axial ratio values, as well as a wide gain bandwidth. This new concept surpasses the traditional LP-CP cells observed in literature, with both outstanding polarization conversion and low losses over a large bandwidth, as elaborated in Section II-B.

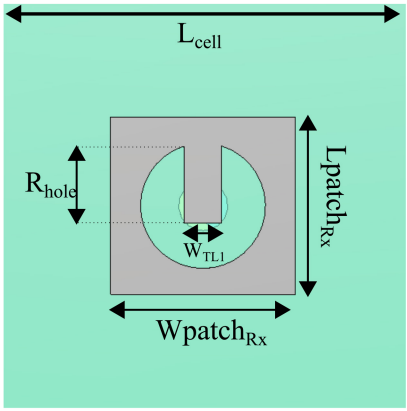

FIGURE 1. Linearly polarized Rx patch antenna.

A. LINEAR TO CIRCULAR UNIT-CELL STRUCTURE, FEEDING ANALYSIS AND PHASE SHIFTING MECHANISM

The unit-cell structure is based on a receiver-transmitter (Rx-Tx) structure. Initially, it consists on a three metallic layer PCB. The Tx and Rx antennas are composed of patches with a central circular slot and microstrip lines connecting them to a centralized via. Both sides of the UC are isolated by the presence of the ground plane, which avoids direct coupling between patches, prioritizes coupling through the metallic via and isolates the polarization of each side, thus enabling the polarization conversion. The Rx patch is detailed in Figure 1. This rectangular patch (dimensions $L_{patchRx} \times W_{patchRx}$) contains one single TL line that connects the circular slot to the central via excitation, the length of this TL is therefore equal to the slot radius R_{slot}. The Rx antenna is linearly polarized, with a straightforward feeding structure that will be further detailed and later generalized for the Tx patch.

The metallic via is the main coupling path between the Tx and Rx antennas, thus the feeding through this structure is the critical design parameter. Patch antennas cannot be fed at the center due to zero input impedance, causing full power reflection. To ensure a proper excitation, circular slots are etched onto the patch surfaces, and the microstrip line functions as a transmission line between the via and the excitation point on the patch antenna. In the case of a lossless situation, the traditional transmission line equations can be employed to compute the input impedance seen by the metallic via, as evidenced by equation (1).

$$Z_{via} = Z_0 \frac{Z_{ant} + jZ_0 tan(\beta R_{slot})}{Z_0 + jZ_{ant} tan(\beta R_{slot})} \tag{1}$$

where Z_0 and β are the microstrip line characteristic impedance and propagation constant, Z_{ant} is the patch antenna input impedance at the excitation point defined by the slot radius R_{slot}. By optimizing the parameters of

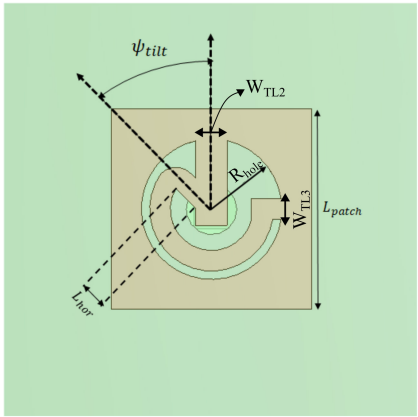

FIGURE 2. Circularly polarized Tx patch antenna, see Table 1 for detailed geometrical parameters.

the transmission line, that is controlling its characteristic impedance and electrical length, it is possible to match the patch antenna impedance to that of the via, thus maximizing the accepted and transferred power. Therefore, the two key geometrical parameters controlling the matching of the structure are the widths (W_{TL}) and lengths (R_{slot}) of the transmissions lines. Furthermore, by modifying the patches lengths (L_{patch}) and widths (W_{patch}) it is possible to define the operating frequency.

This insight of the physical behavior of the UC justifies some of the design choices. First, the use of square patches and circular slots imposes a rotational symmetry around the center of the patch, that is, the patch input impedance Z_{ant} is constant for any feeding point on the circular slot. This ensures that for every rotation ψ of the transmission line, the matching of the structure will not be impacted. Thus, with a single UC design, it is possible to reconstruct any transmission phase state between 0 and 360° by simply rotating the transmission line around the circular slot. Note that only the Tx patch transmission line is rotated, the Rx patches are all identical and polarized on a fixed LP component.

This modeling can be generalized for two simultaneous linear excitations on the Tx side, which physically corresponds to adding a second TL, as depicted in Figure 2. The Tx antenna of the unit-cell is a circular slotted square patch of length $L_{patchTx}$, it contains one vertical TL exciting a first LP mode and a second circularly shaped TL. This additional TL excites a second LP mode that is orthogonal to the first excitation.

In this situation, the validity of the transmission line modeling of the feeding structure persists. However, in this case, two simultaneous impedances are connected to the via excitation. Each of these impedances corresponds to the two orthogonal radiating modes. As a result, the via excitation encounters an equivalent load impedance, which is the parallel combination of these two impedances.

The second excitation is orthogonal to the first one. Furthermore, a phase delay is added through the extension of the second TL in the shape of a circumference arc (inner radius L_{hor}, outer radius $L_{hor} + W_{TL_3}$), in order to keep a constant characteristic impedance. Therefore, by controlling the amplitude balance and the phase delay between LP components, a circularly polarized field can be radiated.

Considering the transmission line (TL) modeling that has been used so far, if a difference in length ΔL is introduced between the two TL, a corresponding phase delay can be calculated by equation (2).

$$\Delta\phi = \frac{2\pi}{\lambda_g}\Delta L \tag{2}$$

where λ_g is the guided wavelength at the TL. To generate a proper CP field, it is required that both LP components must be equal in amplitude and ±90° out of phase. By extending one of the TL of the Tx patch, a modulated phase difference can be achieved between each LP component. The phase delay between LP components is assured by the electrical path difference given by the circular TL increased length compared to the straight line. The phase delay can therefore be controlled by the circular radius of the TL (L_{hor}), and the tilt angle Ψ_{line} that controls the circular arc angle.

Since the microstrip transmission lines that feeds each polarization are no longer identical, the impedances seen by the via excitation are different. Even if the patch access impedance is the same at the end of each line, equation (1) shows that the path length difference will impact the matching of the structure, thus creating an unbalanced excitation of each LP component. Therefore, the design challenge is to respect both amplitude and phase constraints for the CP polarization. To compensate for the path length difference, the characteristic impedance of the TLs must be tailored to impose an equal division of the incoming power. Nevertheless, changing the TLs characteristics will also have impacts on the phase delay between lines, thus the optimization of the structure matching and the UC axial ratio have to be done simultaneously, taking into account the limited space for circular TL given by the slot radius.

The initially proposed structure of Figures 1 and 2 has been simulated and optimized under Floquet modes excitation and periodic boundary conditions. Both patch antennas are etched on a Rogers RO4003C substrate ($\epsilon_r = 3.5$, $\tan\delta = 0.0027$ and thickness 1.52 mm), they are also bonded together with Rogers RO4450F prepeg ($\epsilon_r = 3.52$, $\tan\delta = 0.004$ and thickness 0.1 mm).

The simulations have demonstrated that the initial concept is rather narrowband for a proper CP operation. If the matching bandwidth (S_{11}) is optimized for a larger BW of operation, there is a considerable difference in the amplitude of excitation of each LP component. On the other hand, if the axial ratio of the UC is optimized to achieve a very low level, the corresponding bandwidth is very limited. Figure 3 shows the S-parameters of an UC optimized for a good CP emission at 10.25 GHz. Around this frequency, the two LP components are rather similar with an insertion loss of 0.5 dB, but quickly the transmission coefficient of the

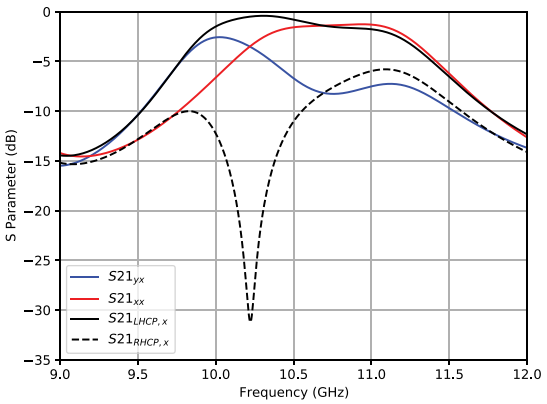

FIGURE 3. Initial LP-CP Unit-Cell S-parameters under normal incidence of Floquet mode.

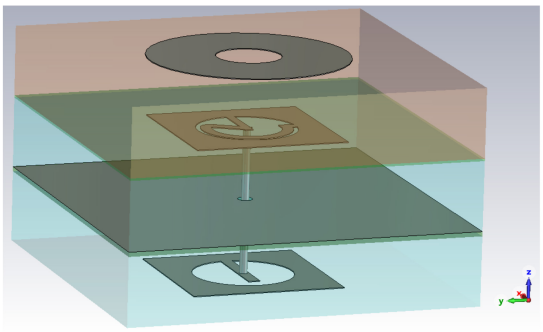

FIGURE 4. Wideband and wide axial ratio unit-cell stack-up with 4 metallic layers and 3 dielectric layers.

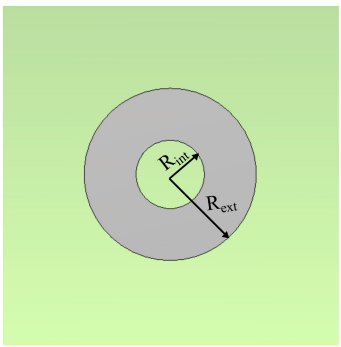

FIGURE 5. Proximity coupled stacked annular ring patch antenna for wideband performance.

polarization fed by the circular TL decreases. Even if the reflection coefficient remains low, the UC will not radiate a CP field as wanted, which can be seen in Figure 7 where a 3 dB axial ratio BW of 2% is achieved.

Although not achieving a large transmission BW, the initial structure demonstrated the validity of the CP generation mechanism. With a reduced footprint, small number of layers and clear insight into the key optimization parameters, this UC can convert the incident LP field into a CP one. The goal of the next section will be to devise a strategy to increase the performance of this structure, to allow wide-band and high efficiency operation.

B. WIDEBAND AND HIGH EFFICIENCY OPERATION

The Tx patch antenna presented in Figure 2 can be considered as a single feed structure, since the same excitation is used to generate both polarizations, even if the access points are different. It is no surprise that this topology is narrowband, as single feed CP antennas are often constrained in axial ratio BW [21].

In order to expand the axial ratio and impedance bandwidth of this UC, a stacked patch configuration is considered for the Tx part of the UC. This technique has been widely used with phased array UCs to broaden the impedance bandwidth, increase the cell gain [22], reduce cross-polarized levels [23] and increase the array field of view [24], [25]. The parasitic element is coupled by proximity to the driven element, thus affecting the impedance seen by the excitation and changing the radiated fields. As explained in [26], this structure can traditionally allow patch antennas to achieve from 15 to 25% impedance matching bandwidth. Traditional parasitic elements include rectangular and circular patches, dipoles, annular or rectangular rings.

The objective of this section is not solely to increase the impedance bandwidth of the UC; rather, the stacked patch configuration is also employed to enhance the radiation of the CP field and improve the current distribution on the driven patch. Accordingly, an annular ring stacked patch is selected as the parasitic element due to its circular symmetry, which allows for easy radiation of the CP field and even excitation of each LP component of the driven patch. The use of an annular ring is preferred over a circular patch as it allows for finer tuning by optimizing both the outer and inner radius.

For larger working BWs, the substrate layer in which lays the stacked patch needs to have a smaller dielectric constant in order to loosely couple the parasitic element [26]. Thus, the upper substrate is selected as a Rogers AD255C layer ($\epsilon_r = 2.55$ and $\tan\delta = 0.0014$). Once the substrate and parasitic element have been chosen, the simulated narrowband UC with performance given by Figure 3 is modified to include the stacked patch. The final stack-up and the stacked patch can be seen in Figures 4 and 5.

The design and optimization procedures for this UC can be synthesized with the following steps:

1) Design a LP-LP UC based on the details of Section II-A. This is a straightforward case, in which very few parameters have to be optimized, since both Tx and Rx patches are identical and square. The key optimization variables are the patch length, the TL width, its length, the ground plane slot hole and inner via diameters. At this stage, the radius of the circular slot plays a crucial role in determining the access impedance of the patch antenna, while parametric studies can be employed to optimize the TL feeding

and achieve maximum transmission bandwidth. It is essential to constrain the size of the ground plane hole to prevent direct coupling between the Tx and Rx sides, a factor that can be verified through simulations of orthogonal phase states of the cells. These simulations should demonstrate closely matched behavior if direct coupling is effectively minimized.

2) Modify the Tx patch antenna to support both vertical and horizontal polarization. Include a second TL and optimize both length and width for a 45° LP in the desired central frequency. For this step, the patch length is already determined by the previous stage, thus only the TL characteristics have to be optimized.
3) Transform one of the TL of the Tx patch into a circular line to extend its length, as in Figure 2. Note that it might be needed to tailor the patch slot radius for increased available space for the circular line. The UC must be optimized for a proper CP emission at the desired central frequency, that means balancing the LP components excitation and imposing the correct phase delay. The key optimization variables are thus the patch slot radius, the straight TL characteristics (length, width), the circular TL line geometry (tilt angle ψ_{line}, radius and width). The central frequency tuning can be achieved by changing the patch length.
4) Include the annular ring stacked patch element, the choice of the upper layer substrate is dependent upon the driven patch substrate dielectric constant. Optimize the outer and inner radius of the annular ring for wide-band axial ratio bandwidth.
5) Finally, a comprehensive optimization of both the driven patch and the stacked patch parameters is performed to improve the impedance matching band-width and transmission coefficients. At this stage, an additional parameter that can be adjusted is the shape of the Rx patch antenna that can be made rectangular, which enhances the matching of the overall structure without impairing the Tx CP performance.

The proposed wideband UC is optimized according to the aforementioned procedure, the key geometrical design parameters can be found in Table 1. Its final S-parameters for a normal incidence of Floquet modes are given in Figure 6, in which the stacked configuration is compared to the initially proposed cell. The resulting structure exhibits a significantly wider bandwidth for the transmission of left-handed circularly polarized signals. In addition, the cross-polarization transmission coefficient is greatly reduced over a much larger frequency range. As a result, it is anticipated that the radiation pattern of this UC will have a higher and more consistent cross-polarization discrimination over the entire simulated frequency band. The insertion loss at the central frequency of 10.5 GHz is only 0.3 dB, while the -1 dB transmission BW is about 13%, throughout this band the difference in transmission between CP components is greater than 15 dB. The far-field components of this UC

TABLE 1. X-band UC key geometrical parameters.

Parameter	Value	Description
L_{Cell}	14.275 mm	Cell periodicity
L_{Patch}	6.13 mm	Tx Patch length
$L_{PatchRx}$	6.13 mm	Rx Patch length
$W_{PatchRx}$	6.13 mm	Rx Patch width
W_{TL_1}	0.46 mm	Rx TL width
W_{TL_2}	0.33 mm	Tx TL width
W_{TL_3}	0.43 mm	Circular TL width
R_{slot}	2 mm	Circular slot radius
L_{hor}	1.2 mm	Inclined line length
Ψ_{tilt}	30°	Line tilt angle
R_{via}	0.16 mm	Central via radius
GND_{hole}	0.3 mm	GND clearance
R_{ext}	4 mm	Stacked patch external radius
R_{int}	1.3 mm	Stacked patch internal radius

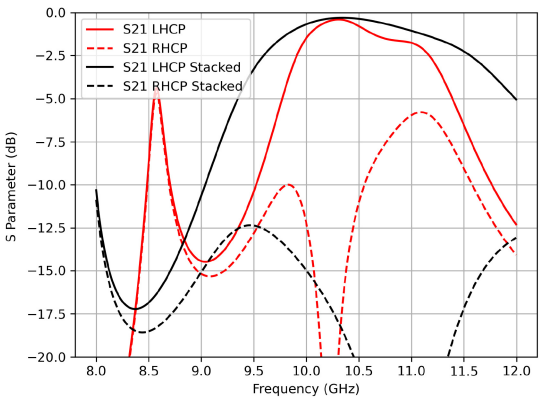

FIGURE 6. Comparison of initial and stacked patch configurations of the LP-CP Unit-Cell at X-band.

are simulated and the extracted axial ratio is showed in Figure 7, it is clear that a much wider and stable AR is obtained. Its value is under 3 dB in a relative BW of about 15%, coincident with the band where a high transmission efficiency is achieved. The radiation pattern of the Tx side of the unit-cell at 10.5 GHz is showed in Figure 8, the cross-polarized level (RHCP) is indeed very reduced and more than 15 dB of XPD is obtained between ±45°. The results confirm that the stacked version of this UC can achieve simultaneously a very high transmission and polarization conversion efficiency.

The phase shifting capabilities of the unit-cell are examined through the phase of the transmission parameter given by the Floquet modes simulation, that is, the correspondence between the rotation of the TLs against the imposed phase shift is observed on Figure 9. It is clear that the 4 phase states shown are uniformly spaced by 90° as the rotation of the TL would impose, furthermore, the phase curves exhibit parallel behavior, with a frequency independent phase difference between states. The transmission parameters absolute value is not affected by these different UC states, the same insertion loss and bandwidths are obtained.

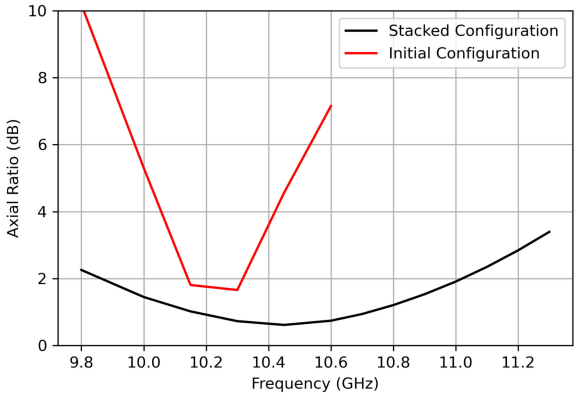

FIGURE 7. Comparison of the initial and the stacked patch axial ratio.

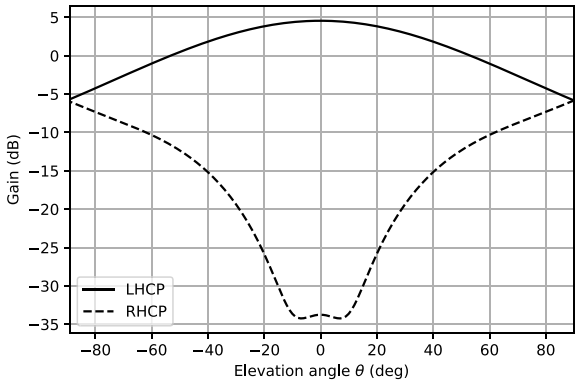

FIGURE 8. Radiation pattern of the Tx circularly polarized stacked patch of the unit-cell at 10.5 GHz, E-plane.

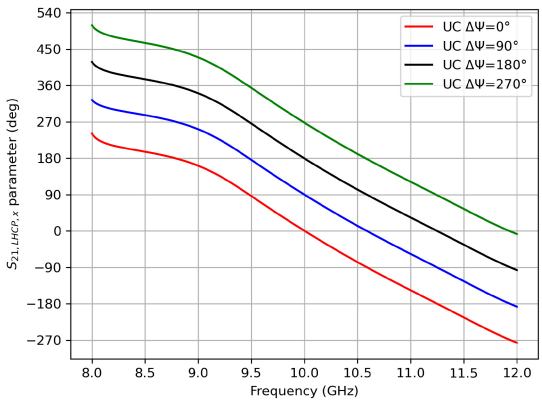

FIGURE 9. Phase response of multiple phase sates of the UC obtained by rotation of the embedded Tx TL.

The performances of the UC are verified against oblique incidence angles, since the majority of the cells in a TA are excited by oblique waves. The S-parameters of the UC for angles up to 30° are showed in Figure 10, the LHCP transmission coefficient remains quite stable throughout the whole bandwidth, with a reduction of the upper frequency band due to the increased coupling between cells. There

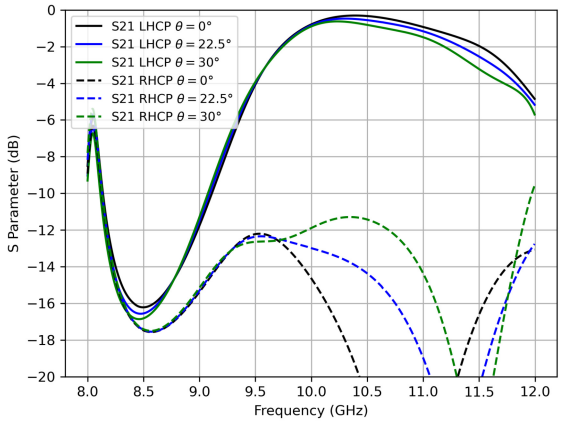

FIGURE 10. LP-CP Unit-Cell S-parameters under oblique incidence of Floquet mode at X-band.

is also an increase in the cross-polarized transmission, but its level remains at least 12 dB inferior to the co-polarized one. At 30° of incidence, the −1 dB transmission bandwidth with axial ratio inferior to 3 dB drops to about 8%. The performance of the cell stays acceptable even for high oblique angles, as the majority of the excitation is concentrated at the center of the array due to the apodization, the cells under high oblique angles contribute little to the final radiation pattern. Thus, by correctly sizing the array dimensions and its focal ratio, the final behavior in terms of polarization purity and BW is expected to be much closer to a normal incidence cell.

C. KA-BAND WIDEBAND UNIT-CELL DESIGN

The excellent performance achieved in the X-band has driven the research towards developing a Ka-band version of this innovative UC. This is motivated by the fact that numerous future applications in Satellite Communications (SatCom), Radars [27], and 5G communications are expected to transition to the millimeter-wave (mmWave) frequency bands to meet the increasing bandwidth demands. Consequently, this UC holds the potential to serve as a high-efficiency circularly polarized antenna in several of these domains. The previous section already demonstrated a quite substantial 1 dB transmission bandwidth with an axial ratio below 3 dB. However, it is worth noting that the total bandwidth can be further expanded by carefully selecting appropriate substrate layers.

For the Ka band version of the UC, the Rogers RO4003C is replaced by the substrate RO3003 ($\epsilon_r = 3$, $\tan\delta = 0.001$ and thickness 0.75 mm) and the AD255C layer is replaced by a Rogers RT5880 ($\epsilon_r = 2.2$, $\tan\delta = 0.0009$ and thickness 0.787 mm). The bandwidth of the UC will be influenced by two significant factors as a result of these modifications. Firstly, it is widely recognized that reducing the dielectric constant of the patch substrate leads to an increased bandwidth [28]. Secondly, the thickness of the substrate has been halved, while the frequency ratio is approximately 3 (30 GHz compared to 10.25 GHz).

TABLE 2. Ka-band UC key geometrical parameters.

Parameter	Value	Description
L_{Cell}	5 mm	Cell periodicity
L_{Patch}	2.37 mm	Tx Patch length
$L_{PatchRx}$	2.15 mm	Rx Patch length
$W_{PatchRx}$	2.25 mm	Rx Patch width
W_{TL_1}	0.45 mm	Rx TL width
W_{TL_2}	0.375 m	Tx TL width
W_{TL_3}	0.25 mm	Circular TL width
R_{slot}	0.835 mm	Circular slot radius
L_{hor}	0.35 mm	Inclined line length
Ψ_{tilt}	45°	Line tilt angle
R_{via}	0.125 mm	Central via radius
GND_{hole}	0.3 mm	GND clearance
R_{ext}	1.26 mm	Stacked patch external radius
R_{int}	0.5 mm	Stacked patch internal radius

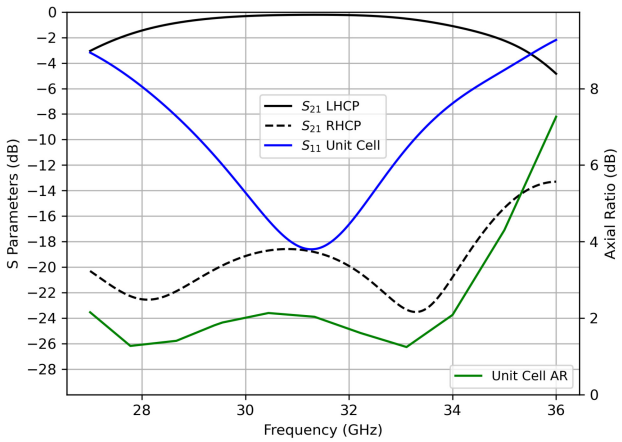

FIGURE 11. Ka-band LP-CP Unit-Cell S-parameters and axial ratio under normal incidence of x-polarized Floquet mode.

Consequently, from an electrical standpoint, the substrates used can be considered thicker, which suggests a wider bandwidth can be anticipated [29].

The key geometrical parameters of the Ka-band version can be found in Table 2. The design and optimization routine are done as described in Section II-B, the S-Parameters of this UC are depicted in Figure 11. The reflection coefficient S_{11} is smaller than -10 dB from 28.8 to 33.5 GHz, corresponding to a relative frequency bandwidth of roughly 15.7%. The most important parameter is the transmission towards the CP components, the picture shows a minimum insertion loss of only 0.2 dB at 30 GHz, furthermore the transmission coefficient is higher than -1 dB from 28.4 to 33.8 GHz, which is equivalent to a 18% relative BW. The cross-polarization transmission levels are very reduced throughout the whole simulated band, it is possible to see that from 27 to 34 GHz (23% relative BW) there is more than 18 dB difference between the transmission of each CP component.

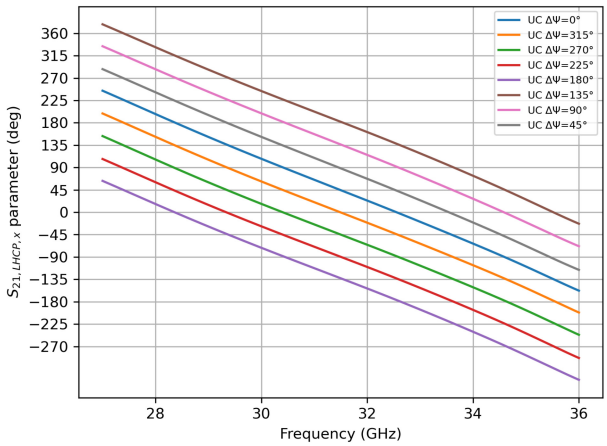

FIGURE 12. Phase response of multiple phase sates of the Ka-band UC obtained by rotation of the embedded Tx TL.

The high isolation between CP components demonstrated by the S-parameters is directly related to the axial ratio of the emitted fields of this UC. The UC simulated radiation pattern is obtained and the corresponding axial ratio depicted on Figure 11. The AR is under 2 dB from 27 to 34 GHz, which in itself is representative of a 23% relative BW. Nevertheless, if the -1 dB transmission criteria is also considered the simultaneous high transmission and polarization conversion efficiency relative BW is roughly 18%. This criteria is somewhat highly restrictive, since excellent CP fields and high radiation efficiencies are required simultaneously, thus the cell is capable of excellent performances given the wide-band behavior demonstrated. It is important to note that this performance is superior to all previously published LP-CP transmitarray UCs. The novel cell is capable of respecting both constraints over a larger bandwidth than all the works of Table 3, in which a comprehensive comparison between different UCs is demonstrated. The proposed concept does not seek to be low profile, since it possess 3 substrate layers, but still its size and thickness align with current state of the art practices, with a profile inferior to 0.25λ.

The phase shifting response of the Ka-band version of the UC is analogous to the X-band one, as depicted by Figure 12. The simulations show that even for higher quantizations, the correspondence of the TL rotation angle and the imposed phase shift are respected, in this case, the 8 states of a 3-bit quantization are showed. A uniform and frequency independent phase difference of 45° is observed between each successive state. In reality, any quantization could be realized with this structure, without the need to re-optimize the UC structure.

The angular stability of the UC under oblique incidence angles has been assessed through simulations, and the corresponding S-parameters are illustrated in Figure 13. The simulation results demonstrate that the UC performance remains practically unaffected by incidence angles up to 20°. Even at a 30° incidence, the cross-polarized levels remain at least 15 dB lower than the co-polarized levels, and the

TABLE 3. Comparison of LP-CP unit-cell intrinsic performances.

Ref	Freq (GHz)	Structure	Size (λ_0^2)	Profile (λ_0)	IL (dB)	BW $S_{21} > -1$ dB (%)	BW AR < 3 dB (%)	3dB Loss from SR[a]
[8]	20	Dual C-shaped slot circular patches	0.38x0.38	0.2	0.2	15	LP Cell	Yes
[30]	60	Offset pin feed patch	0.5x0.5	0.10	0.35	6.50	LP Cell	Yes
[9]	28	Magnetoeletric dipole	0.47x0.47	0.39	0.6	30	Elliptical Pol.	Yes
[11]	10	Circular patch with asymmetrical slot	0.47x0.47	0.1	0.17	11	N.A[b]	No
[31]	30	Elliptical dielectric resonator	0.5x0.5	2.34	0.2	13	17	No
[13]	30	Truncated corner patch	0.5x0.5	0.10	0.9	10	1	No
[32]	30	Reconfigurable LP-CP Polarizer	0.51x0.51	0.25	0.7	6.9	14	No
This Work	10 30	TL feed CP Stacked Patch	0.5x0.5 0.5x0.5	0.16 0.24	0.3 0.2	13 18	16 25	No

a: Sequential Rotation; *b*: Not Available;

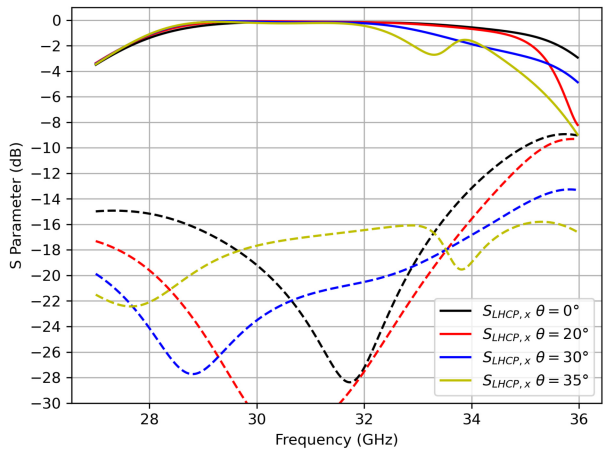

FIGURE 13. LP-CP Ka-Band unit-cell S-parameters under oblique incidence of Floquet mode.

transmission bandwidth (BW) exceeds 16%. However, for larger incidence angles, the upper limit of the transmission BW starts to significantly deteriorate. When the incidence angles exceed 45°, the BW diminishes to less than 10%. Notably, the Ka-band version of the UC exhibits enhanced angular stability compared to the X-band version. A 45° maximal incidence angle corresponds to a focal ratio of 0.5, therefore even for low-profile designs the UC is expected to outperform most of the previously published works.

To showcase the effectiveness of the UC, several transmitarray (TA) designs have been implemented to evaluate the performance of the UC in various configurations. Section III provides a comprehensive explanation of the TA antenna designs in both X-band and Ka band. Initially, X-band prototypes are employed as proof-of-concept, serving to illustrate the advantages of designing a high-efficiency LP-CP UC compared to previous approaches utilizing sequential rotation. Once the concept's viability is established, a significantly larger TA aperture in the Ka-band consisting of 4900 unit-cells is designed, simulated, and verified through measurements. This aperture achieves an impressive gain of approximately 40 dB and exhibits very low axial ratio, making it suitable for satellite communication (SatCom) applications in the mmWave band.

III. TRANSMITARRAYS DESIGN, SIMULATION AND MEASUREMENTS

Once the optimization of the UCs is finished, the synthesis of high gain and circularly polarized TAs is performed by means of semi-analytic simulations and full-wave solvers. The methodology applied is the same as in [18]. In brief, the UC radiation pattern and S-Parameters are extracted from the periodic boundary simulations and they are used to model the whole TA aperture using the hybrid code [33]. This semi-analytic tool allows the fast and precise simulation of the antenna, thus permitting comprehensive studies of quantization losses, spill-over losses, feed choice and positioning. Once the results of these first simulations are satisfactory, full-wave simulations are used to obtain the final behavior of the antenna including complex phenomena not modeled by the hybrid code, such as edge diffraction and finite array effects. On this study multiple full-wave strategies have been used, notably CST Microwave Studio (MWS), Ansys-HFSS and ONERA's HPC solver FACTOPO [19], [34].

A. X-BAND PROOF-OF-CONCEPT CP TRANSMITARRAY

The 16 dB gain horn feed and the 0.75 focal ratio utilized in previous works [18], [35] are maintained to establish a

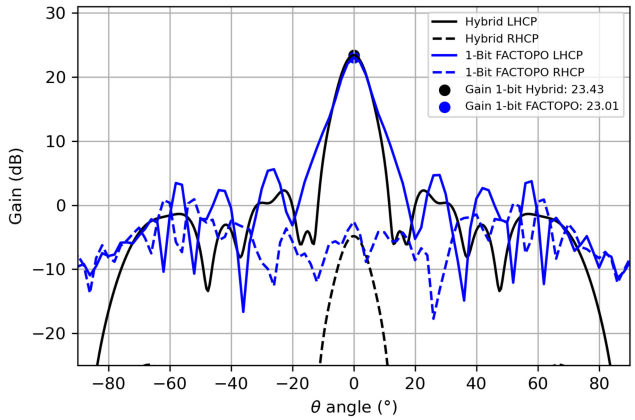

FIGURE 14. Simulated Radiation Pattern of a 1-Bit Circularly polarized X-band TA, E-Plane, 10.5 GHz.

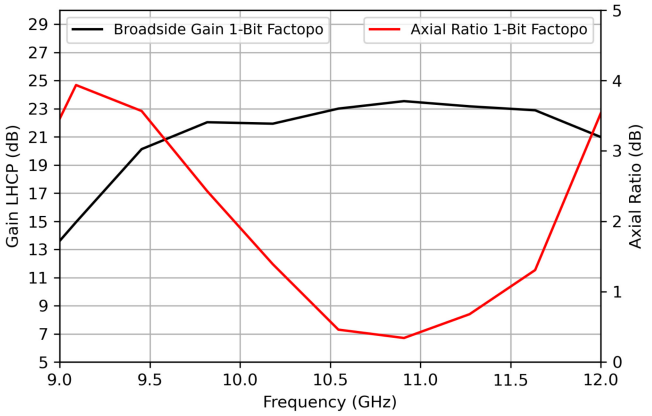

FIGURE 15. Simulated axial ratio and gain bandwidths of the 1-Bit X-band CP TA.

TABLE 4. Hybrid simulation results of the quantization impact over the X-band TA performances.

Number of Bits	1-bit	2-bit	3-bit	4-bit
Gain (dB)	24.46	26.64	26.78	27.1
Axial Ratio (dB)	0.5	0.18	0.1	0.2
SLL (dB)	18	30	32	34

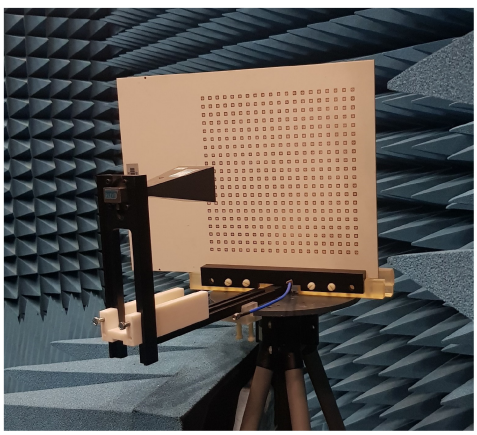

FIGURE 16. Measurement of the proof-of-concept X-band 2-bit CP TA.

convenient benchmark for comparison. For the same reason, a 20 × 20 cells TA aperture is considered, the cell length is 14.275 mm and thus the aperture diameter is 285.5 mm. The hybrid code is employed to assess the influence of phase quantization on the performances of the TA. This evaluation encompasses both gain and polarization conversion.

Initially, a 1-bit quantization is employed to examine the inherent polarization conversion performance of the UC, disregarding any effects caused by geometrical phase rotation.

Figure 14 illustrates a comparison of the radiation pattern of the TA obtained with hybrid and full wave simulations conducted with FACTOPO. The co-polarization pattern exhibits substantial agreement between the two simulations, but due to the limitations of the hybrid code, the finer details such as the SLL values and null positions are slightly shifted compared to the full-wave solver, see [18] for detailed information. Nevertheless, the main lobe is well predicted by both results for the two CP components. A cross-polarization discrimination (XPD) superior to 25 dB is observed between the LHCP and RHCP fields, indicating that even with a 1-bit design, excellent circular polarization performance can be achieved, which is a key differential to all works on Table 3 that necessarily need two or more bits of quantization for proper CP performances. As the novel UC itself has great CP conversion capabilities, no additional strategies are needed for wideband performance. The obtained axial ratio and gain bandwidth are showed in Figure 15, there is a gain shift towards higher frequencies as the peak gain of 23.6 dB is around 10.9 GHz. The 3-dB axial ratio BW is from 9.6 to 11.8 GHz, or 20% relative band.

The analysis is further expanded for higher numbers of bits of quantization, in order to determine the optimal performances of the finite size TA antenna. Table 4 shows the obtained results for a variety of number of quantization bits at 10.5 GHz, two important effects are to be observed. First, as the number of bits increases the phase error is reduced and thus the broadside gain is maximized, while the SLLs are minimized. The second effect is mainly concerning the cross-polarization discrimination (XPD), for a 1-bit quantization the axial ratio is 0.5 dB. For higher quantizations, the XPD is improved by the smaller phase errors and the rotational symmetry of the phase correction, which aids to expand the transmitarray axial ratio BW further than the UC's own BW. The phase rotation scheme improves the XPD by imposing opposite phase responses to the LHCP and RHCP fields, due to the Pancharatnam–Berry phase phenomenon.

A 2-bit quantization is kept for the final design, given the minimal 0.6 dB gain increase observed between 2 and 4-bit quantization. The lower quantization simplifies the analysis and comparison to the 2-bit sequentially rotated TA of [35]. Note that this is purely a choice for comparison reasons. For a final antenna seeking the maximum performances a higher number of bits could be chosen without any additional

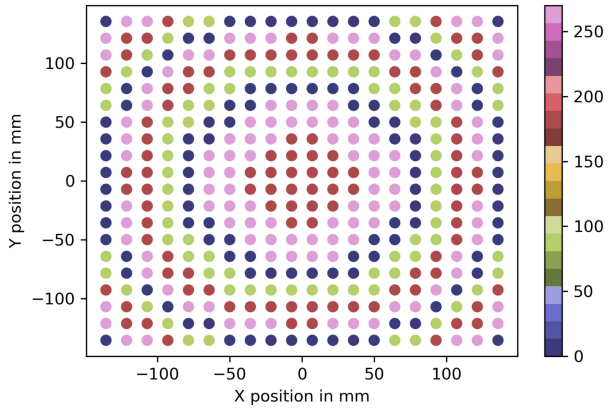

FIGURE 17. 2-Bit phase correction distribution for a broadside gain peak at 10.25 GHz.

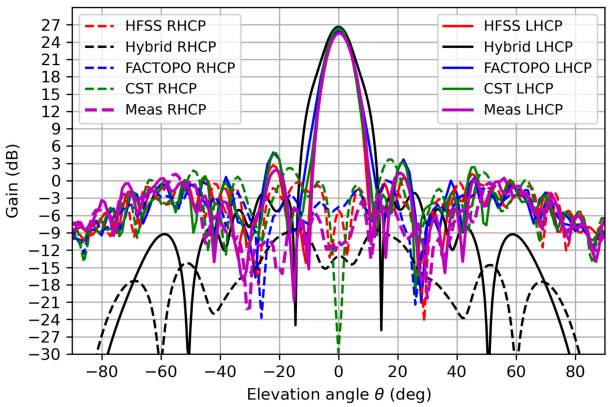

FIGURE 18. Simulated and measured radiation pattern of 2-bit X-band TA in circular polarization, E-Plane, 10.5 GHz.

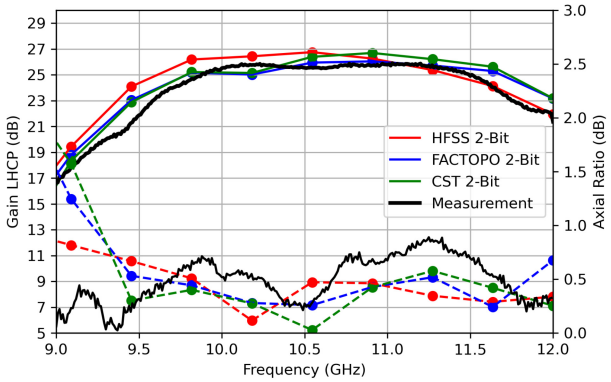

FIGURE 19. Simulated and measured axial ratio and gain bandwidth of 2-bit X-band TA in circular polarization.

difficulties in the design, since each phase state is obtained by simple rotation of the Tx patch transmission lines.

A 20 × 20 transmitarray (TA) is designed to have its main beam pointing in the broadside direction, with a centralized focal source excitation. The chosen focal distance is approximately 214 mm, striking a balance between the antenna profile and its aperture efficiency, considering the high gain of the focal source. To ensure accuracy, the antenna is simulated using multiple full-wave solvers. The phase correction distribution over the TA aperture can be seen in Figure 17.

The measured radiation pattern of the fabricated transmitarray (TA) is compared to the simulated results, as depicted in Figure 18. The co-polarized component shows excellent agreement between simulations and measurements, with the overall shape of the pattern closely resembling each other. The simulated mean LHCP gain is approximately 26.2 dB, while the measured gain is 25.6 dB, resulting in a measured aperture efficiency of 30% (compared to the simulated 33%). The slight difference in gain can be attributed to fabrication tolerances and alignment issues between the feed and the aperture during measurements.

However, there are notable discrepancies in the cross-polarization behavior predicted by the simulations. This can be attributed to the different numerical methods employed by each solver, such as variations in meshing convergence criteria and mathematical schemes. These differences may explain the observed variations in the broadside behavior of the transmitarray. Nevertheless, both simulations and measurements agree that there is significant discrimination between the CP components at broadside, with a measured XPD exceeding 35 dB. Moreover, the radiation pattern of the cross-polarized component shows excellent agreement for off broadside angles.

The bandwidth characteristics of the transmitarray (TA) are illustrated in Figure 19. There is a high degree of agreement among all the full-wave solvers and the measured results. The measured peak gain is 25.6 dB at a frequency of 10.25 GHz, which aligns closely with the results from FACTOPO. Although HFSS and CST slightly overestimate the gain by approximately 0.9 dB, this difference is acceptable considering the fabrication tolerances and measurement uncertainties involved. The measured −1 dB gain bandwidth spans 16% of the operating frequency range, while the 3 dB axial ratio bandwidth exceeds 30%. Notably, the axial ratio values remain below 1 dB throughout the entire measured band, with a minimum value of 0.25 dB at the central frequency. This demonstrates exceptional circular polarization (CP) performance.

The comparison between the 2-bit circularly polarized (CP) transmitarray (TA) and the sequentially rotated CP TA from [35], shown in Figure 20, highlights three major advantages of using true CP UCs. Firstly, the aperture efficiency is effectively doubled by eliminating the 3 dB polarization conversion losses. Secondly, the obtained axial ratio is more stable and exhibits significantly smaller values. Lastly, the gain bandwidth is expanded. The 2-bit X-band TA effectively demonstrates the superior efficiency of true LP-CP wideband UCs, showcasing their benefits over sequentially rotated LP-CP TAs.

To achieve higher aperture efficiency, a better choice of feed is crucial. Indeed, using a 16 dB gain horn as a feed

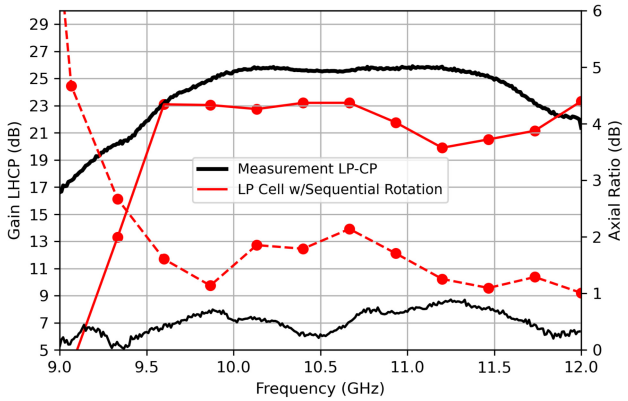

FIGURE 20. Comparison between the sequential rotation technique and the true LP-CP unit-cell transmitarray gain and AR performances.

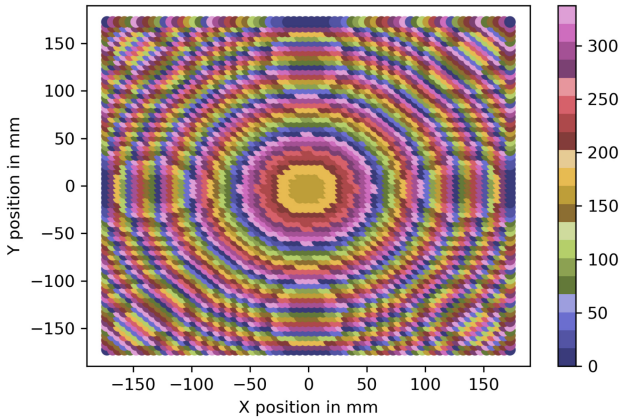

FIGURE 21. 4-Bit phase correction distribution for a broadside gain peak at 29 GHz.

imposes a high focal ratio requirement to ensure proper apodization. A compromise value of 0.75 was selected, considering the trade-off between the antenna form factor and the aperture efficiency. Simulations indicate that by increasing the focal ratio and the number of bits, aperture efficiency exceeding 40% can be achieved. Alternatively, selecting a lower gain focal source would also allow for smaller focal ratios to deliver similar performance. This valuable insight will be exploited in the design of highly efficient and high-gain antennas with excellent CP characteristics in the Ka-band TA designs.

B. KA-BAND PROOF-OF-CONCEPT CP TRANSMITARRAY

The successful optimization of the UC in the Ka-band has inspired the design of highly efficient TA antennas. These antennas are particularly important for applications such as base station SatCom antennas and 5G mmWave backhauling, where high-gain antennas are essential to ensure sufficient data throughput, especially considering the increased losses associated with propagation at these frequencies. In this design case, the objective is to achieve a 40 dB gain antenna to meet the requirements of common SatCom applications. Additionally, it is crucial to have an axial ratio below 1 dB across the entire bandwidth to minimize interference with other systems. These design considerations aim to develop high-performance TA antennas suitable for demanding communication applications.

Due to limitations in the availability of wideband sources in the Ka-band, the choice of feed for the TA was constrained. The only available option was a 16 dB gain LP horn antenna. To minimize costs associated with ordering or designing and fabricating a more suitable source, the LP horn antenna was selected as the feed for the TA. As explained, this choice will be reflected on the focal ratio chosen for the TA.

The aperture size to obtain a 40 dBi gain antenna can be estimated through the definition of aperture efficiency of a $N \times N$ TA, by taking in consideration the spillover losses and focal ratio. These parameters are optimized using the hybrid semi-analytical tool [33] and a array size of 70×70 cells is fixed. A focal ratio of about 0.82 selected as a compromise between the antenna profile and the aperture efficiency, thus the focal distance F is fixed at 300 mm.

Consequently, a TA consisting of 4.900 cells was designed and simulated using the FACTOPO full-wave solver. A 4-bit quantization is used to maximize the aperture efficiency and the phase correction distribution over the TA aperture can be seen in Figure 21. The simulation of such a large-scale problem requires the utilization of the domain decomposition method (DDM). This approach is crucial due to the presence of thousands of subwavelength UCs and a significant air gap between the feed source and the TA aperture. The DDM enables the solution of this multiscale problem in a much more efficient manner, as it eliminates the need to construct a global mesh for the entire problem. Instead, each subdomain is solved on a single core within a massive CPU cluster. For more detailed information, refer to [19], [34]. The computation of the radiation pattern using the chosen approach still proved to be highly challenging. It required a substantial computational resource, with a total of 16,429 CPU cores being utilized. It is worth noting that the virtual mesh used in the computation consisted of a staggering 2.7 billion unknowns. Despite the complexity of the problem, the time required per frequency point was approximately 35 minutes, which is significantly lower than the time required by HFSS and CST for smaller problems. This highlights the efficiency and effectiveness of the chosen approach in handling such demanding simulations.

The radiation pattern of the proposed transmitarray (TA) at 29 GHz is presented in Figure 23, showing excellent agreement between simulations and measurements for the copolarization. The measured peak gain of 39.43 is only 0.1 dB lower than the simulated value obtained using FACTOPO. The overall shape of the radiation pattern closely matches the simulations, accurately predicting the location and peak values of the side lobes. The first side lobe level (SLL) is at -27 dB. While the simulations indicated a discrimination of over 40 dB between CP components,

TABLE 5. Comparison of LP-CP transmitarray performances.

Ref	Freq. (GHz)	Source Antenna	Gain (dB)	Number of Elements	1 dB Gain BW (%)	3 dB AR BW (%)	Ap. Eff. (%)
[8]	20	10 dB LP Horn	26	30×30	15	20	24
[30]	60	10 dB LP Horn	23	20×20	17	30	16
[9]	28	10 dB LP ME Dipole	21.5	18×18	26	40.7	25
[11]	10	5 dB LP Patch	21.8	20×20	6	20	12[a]
[31]	30	16 dB LP Horn	26	16×16	13.3	17	40
[13]	30	10 dB LP Horn	33.5	40×40	10	16.67	47
[17]	30	10 dB LP Horn	26.9	24×24	11.6	N.A[b]	25
This Work	10	16 dB LP Horn	25.6	20×20	16	30[c]	30
	30		39.4	70×70	8	26.67[c]	55

a: Estimated by peak gain and aperture size; *b*: Not Available; *c*: Refers to AR $\leq$ 1 dB[c]

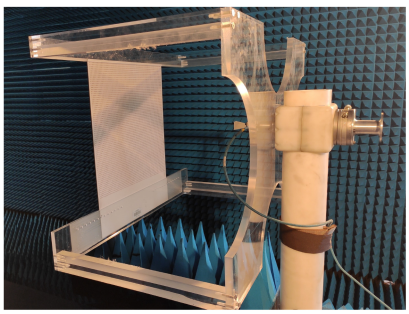

FIGURE 22. Measurement of the proof-of-concept 4-bit Ka-band CP TA.

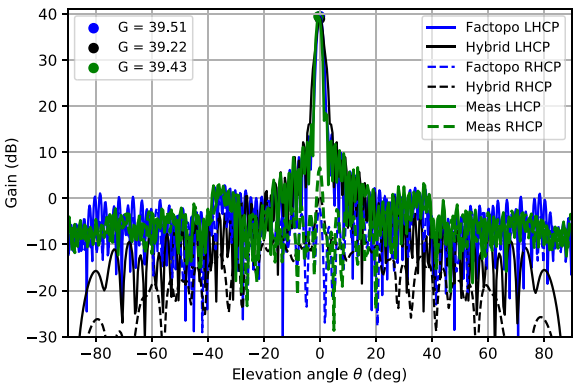

FIGURE 23. Simulated and measured radiation pattern of 4-bit Ka-band CP TA, E-Plane, 29 GHz.

the measured value is approximately 32 dB. Given the challenges of measuring antenna patterns at the Ka-band, obtaining a measured axial ratio of 0.5 dB can be considered a very good match to the simulated value of 0.2 dB. The measured peak aperture efficiency is 55%, surpassing previous LP-CP implementations. The breakdown of the measured TA antenna is given on Table 6, in which the ideal directivity is calculated by the aperture size given a uniform excitation of all elements. The spillover, taper and quantization losses are computed as detailed in [36].

Table 5 shows a comparison of multiple LP-CP TA previously mentioned. The proposed UCs allows at the same time to achieve larger gain and axial ratio bandwidths with improved aperture efficiency.

TABLE 6. Loss budget of the measured Ka-band CP TA.

Ideal Directivity	41.87 dB
Spillover Loss	1 dB
Taper Loss	0.9 dB
Quantization Loss	0.1 dB
Insertion Loss, dieletric and conductive losses	0.16 dB
Losses from fabrication and measurement errors	0.21 dB
Measured Gain	39.5 dB

While the design primarily targets fixed beam applications, some degree of beam-steering may be necessary to adapt the network link to changing conditions, such as antenna alignment due to mechanical constraints or relative movement between stations. A commonly used method to achieve beam scanning with passive transmit-array (TA) antennas involves mechanically shifting the focal source along a specified axis, thereby inducing a phase gradient and steering the beam. However, this method has drawbacks, as the phase correction is not precisely calculated for multiple source positions, leading to higher-order terms in the phase correction that generate increased side lobes and scan loss.

The TA support depicted in Figure 22 allows for horizontal displacement of the TA lens, with a maximum displacement of 80mm. Figure 24 illustrates a scanning range of $\pm 16.5°$; since the behavior is symmetric, only the negative scan is shown. The maximum scan loss is 3 dB, and the sidelobe levels (SLLs) peak at -11 dB at -16.5°. Although the scan range is smaller compared to phased arrays, the beam-steering method is cost-effective and consumes less power. Furthermore, TA antennas offer superior radiation efficiency compared to phased arrays, particularly when scaling antenna designs to accommodate a large number of elements such as a 4900 array. Even if one were to employ a passive BFN with a cooperative feed network for a fixed beam direction, the accumulated losses on the transmission lines used to feed each element at its designated position increase both in frequency and with the

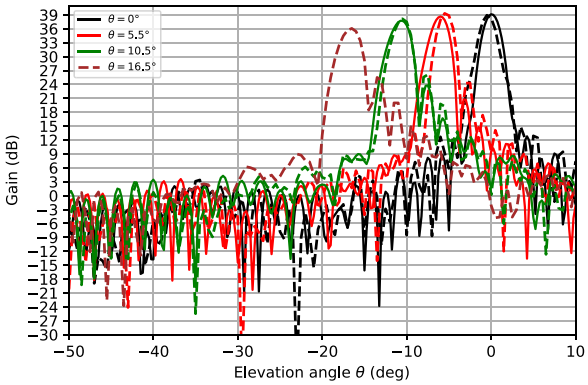

FIGURE 24. Mechanical beam-steering of the 40 dB TA antenna by lateral displacement of the lenses. Solid lines corresponds to full-wave simulations with FACTOPO, while dashed lines corresponds to measurements. Plan E, 29 GHz.

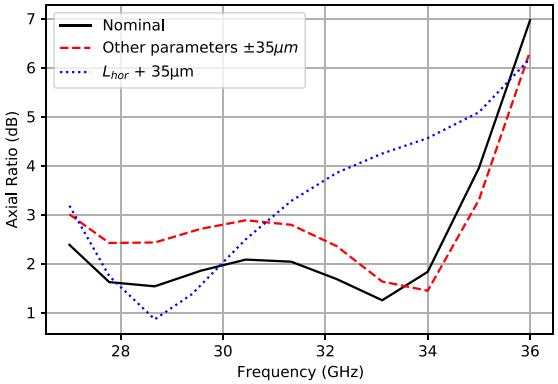

FIGURE 25. Impact of fabrication tolerances over the unit-cell axial ratio.

number of elements. This occurs because the lines continue to elongate in physical and electrical length, as shown in [37]. The achieved scan range meets the requirements of GEO communications and 5G backhauling links.

The proposed work stands out in comparison to the references listed in Table 5. The X-band version achieves higher gain bandwidths than most of the existing works, indicating its suitability for a wide range of applications. Additionally, when compared to the designs that offer larger bandwidths, the X-band version demonstrates superior aperture efficiency. Furthermore by employing a more suitable feed choice, further enhancements in aperture efficiency could be achieved. The smaller gain bandwidth observed in the Ka-band version is attributed to its considerably larger aperture size. In this case, the gain bandwidth is limited by phase correction error rather than the performance of the individual UCs, advanced phase correction synthesis could be used to increase the bandwidth [38]. Despite this limitation, the Ka-band design still achieves significant improvements in aperture efficiency compared to previous works. This highlights the importance of considering the trade-off between aperture size, gain bandwidth, and overall performance when designing transmitarray antennas for different frequency bands. These findings emphasize the notable performance of the proposed design and its potential for delivering efficient and high-gain solutions with excellent CP performance.

C. FABRICATION TOLERANCES AND SCALABILITY

A 70x70 panel has been successfully fabricated using standard multilayer PCB fabrication techniques. The primary fabrication challenge being the metallization of the inner vias. This issue can be mitigated by selecting easily metallized materials such as the Rogers RO4003. The track widths are maintained at over 200μ, well above current fabrication minimum tolerances. For larger panels, assembly via multiple sub-panels containing smaller arrays, akin to deployable multi-facet antennas, is feasible.

The second challenge arises from variations in geometrical parameters due to tolerance in copper etching, typically characterized by a standard deviation of $\pm 35\mu m$ in standard procedures. A tolerance study conducted on key parameters reveals minimal impact on the unit-cell performance for most parameters, except for the length L_{hor}. In the X-band version of the unit cell, results are notably more stable due to smaller deviations compared to its geometrical sizes. Therefore, only the Ka-band results are detailed here.

Given that the axial ratio bandwidth is a primary concern in this design, Figure 25 illustrates the variation of this parameter with unit-cell tolerance. It indicates that the worst-case scenario for geometrical variations, excluding L_{hor}, results in a roughly 1 dB increase in the axial ratio, which remains below the 3 dB threshold and thus does not significantly impact the cell's design. However, the most critical variation occurs with the maximum deviation of the L_{hor} parameter, leading to a significant reduction in the axial ratio bandwidth. While this would have a considerable impact on a 1-bit design, passive designs can mitigate this impact by exploiting higher quantizations. The demonstration of the 4900-cell array exhibits excellent agreement with simulations and demonstrates very low levels of cross-polarization, confirming the feasibility of the design.

However, fabrication challenges may arise for frequencies higher than the Ka band due to space limitations within the patch for accommodating curved transmission lines, but these cases are out of the scope of this paper.

Therefore, the versatility of the design finds applications across various communication domains, catering to high-speed point-to-point communication hotspots for very high speed Internet access, facilitating 5G backhauling infrastructure due to increased radiation efficiency and smaller polarization mismatch losses, and enhancing connectivity in GEO satellite communications due to precise beam-shape, low cross-polarized lobes and small SLL. These applications underscore the adaptability and effectiveness of the technology in meeting the evolving demands of modern telecommunications, ensuring robust and efficient data transmission over vast distances and challenging environments.

IV. CONCLUSION

This work presents a novel UC design for linear to circular polarization (LP-CP) conversion in transmitarray antennas. The proposed concept incorporates a transmission line modeling-based excitation technique for wideband patch antennas, enabling the radiation of a wideband CP field with a very low axial ratio. The LP-CP conversion mechanism introduced in this study represents a significant departure from previous realizations and has not been previously published. To further enhance the bandwidth and transmission efficiency, a stacked patch approach is employed, resulting in simultaneous high polarization conversion and transmission efficiency. The UC design methodology is comprehensively described, and its effectiveness is demonstrated through the realization of two transmitarray designs in X and Ka bands.

Experimental results from a fabricated X-band prototype with a 20×20 cell configuration showcase a peak aperture efficiency of 30%, accompanied by a simultaneous 16% -1 dB gain and 1 dB axial ratio bandwidths. Furthermore, a wideband and highly efficient transmitarray operating in the Ka band, composed of a 70×70 cell array, is designed, fabricated, and measured. This array achieves an impressive gain of 39.8 dB at 29 GHz, corresponding to an aperture efficiency of 55%, surpassing previous realizations of LP-CP transmitarray antennas. Additionally, the axial ratio values remain below 0.5 dB, demonstrating excellent gain and polarization purity.

The remarkable performance of the Ka-band prototype makes it suitable for future millimeter-wave link applications demanding high data rates. Further research directions include the optimization of feed selection and the implementation of conformal transmitarray designs to reduce antenna profiles and enhance gain bandwidth in high-gain applications. Furthermore, the development of multi-beam and multi-band transmitarrays will be studied for space communications systems.

REFERENCES

[1] C. Jouanlanne et al., "Wideband linearly polarized transmitarray antenna for 60 GHz backhauling," *IEEE Trans. Antennas Propag.*, vol. 65, no. 3, pp. 1440–1445, Mar. 2017.

[2] L.-H. He, Y.-L. Ban, and G. Wu, "Dual-band quad-polarized transmitarray for 5G mm-wave application," *IEEE Access*, vol. 9, pp. 117520–117526, 2021. [Online]. Available: https://ieeexplore.ieee.org/document/9521167/

[3] G. Amendola et al., "Low-earth orbit user segment in the ku and Ka-band: An overview of antennas and RF front-end technologies," *IEEE Microw. Mag.*, vol. 24, no. 2, pp. 32–48, Feb. 2023.

[4] T. Freialdenhoven, M. Schepers, and T. Dallmann, "Frequency controlled polarization rotating transmitarray for polarimetric radar applications," in *Proc. 52nd Eur. Microw. Conf. (EuMC)*, Sep. 2022, pp. 660–663.

[5] X. Ding et al., "Metasurface holographic image projection based on mathematical properties of fourier transform," *PhotoniX*, vol. 1, no. 1, p. 16, Jun. 2020. [Online]. Available: https://doi.org/10.1186/s43074-020-00016-8

[6] C. Dehos, J. L. González, A. De Domenico, D. Kténas, and L. Dussopt, "Millimeter-wave access and backhauling: The solution to the exponential data traffic increase in 5G mobile communications systems?" *IEEE Commun. Mag.*, vol. 52, no. 9, pp. 88–95, Sep. 2014.

[7] *Fixed Radio Systems; Characteristics and Requirements for Point-Topoint Equipment and Antennas*, European, Standard ETSI EN 302 217, Jan. 2012.

[8] S. Yang, Z. Yan, P. Liu, and X. Li, "A linearly-polarized-feed dual-circularly polarized dual-beam transmitarray with independent beam control," *IEEE Antennas Wireless Propag. Lett.*, vol. 21, pp. 1497–1501, 2022. [Online]. Available: https://ieeexplore.ieee.org/document/9766446/

[9] J. Hu, H. Wong, and L. Ge, "A circularly-polarized multi-beam magneto-electric dipole transmitarray with linearly-polarized feeds for millimeter-wave applications," *IEEE Trans. Antennas Propag.*, vol. 70, no. 7, pp. 6012–6017, Jul. 2022.

[10] T.-J. Li, G.-M. Wang, J.-G. Liang, and H.-P. Li, "A method for transmitarray antenna profile reduction based on ray tracing principle," *IEEE Antennas Wireless Propag. Lett.*, vol. 21, pp. 2542–2546, 2022.

[11] T.-J. Li, G.-M. Wang, H.-P. Li, and H.-S. Hou, "Circularly polarized double-folded transmitarray antenna based on receiver-transmitter metasurface," *IEEE Trans. Antennas Propag.*, vol. 70, no. 11, pp. 11161–11166, Nov. 2022. [Online]. Available: https://ieeexplore.ieee.org/document/9827939/

[12] H. Lei, Y. Liu, Y. Jia, Z. Yue, and X. Wang, "A low-profile dual-band dual-circularly polarized folded transmitarray antenna with independent beam control," *IEEE Trans. Antennas Propag.*, vol. 70, no. 5, pp. 3852–3857, May 2022. [Online]. Available: https://ieeexplore.ieee.org/document/9611077/

[13] F. Diaby et al., "Wideband circularly-polarized 3-bit transmitarray antenna in Ka-band," in *Proc. 11th Eur. Conf. Antennas Propagat. (EUCAP)*, 2017, pp. 2269–2273.

[14] P. Naseri, S. A. Matos, J. R. Costa, C. A. Fernandes, and N. J. G. Fonseca, "Dual-band dual-linear-to-circular polarization converter in transmission mode application to *K*/*Ka*-band satellite communications," *IEEE Trans. Antennas Propag.*, vol. 66, no. 12, pp. 7128–7137, Dec. 2018.

[15] J. Lundgren, O. Zetterstrom, F. Mesa, N. J. G. Fonseca, and O. Quevedo-Teruel, "Fully metallic dual-band linear-to-circular Polarizer for K/Ka-band," *IEEE Antennas Wireless Propag. Lett.*, vol. 20, pp. 2191–2195, 2021.

[16] I. Derafshi and N. Komjani, "A new high aperture efficiency transmitarray antenna based on huygens metasurfaces," *IEEE Trans. Antennas Propag.*, vol. 70, no. 7, pp. 5458–5467, Jul. 2022.

[17] A. Clemente, R. Madi, F. F. Manzillo, M. Smierzchalski, J. Reverdy, and R. Sauleau, "Reconfigurable transmitarrays at Ka-band with beam-forming and polarization agility," in *Proc. 17th Eur. Conf. Antennas Propagat. (EUCAP)*, 2023, pp. 1–5.

[18] J. Pages-Mounic, A. De Oliveira Cabral Junior, A. Barka, and H. Kaouach, "Hybrid numerical methodology for efficient design and optimization of transmit-array antennas, X-band application," *IEEE Access*, vol. 9, pp. 148302–148314, 2021.

[19] A. Barka, S. A. Matos, J. R. Costa, C. A. Fernandes, and H. Chreim, "Applying massively parallel computing to multiscale Ka dual-band transmit-array analysis using FETI-2LM," *IEEE J. Multiscale Multiphys. Comput. Techn.*, vol. 5, pp. 235–244, 2020.

[20] A. Barka, S. Matos, J. R. Costa, and C. A. Fernandes, "Assessment of FETI DDM methodologies for the simulation of high gain Ka-band transmit arrays," in *Proc. Int. Symp. Antennas Propag. (ISAP)*, 2017, pp. 1–2.

[21] A. Raeesi, H. Al-Saedi, W. M. Abdel-Wahab, S. Gigoyan, and S. Safavi Naeini, "Ka-band circularly-polarized antenna array with wide gain and axial ratio bandwidth," in *Proc. 15th Eur. Conf. Antennas Propag. (EuCAP)*, 2021, pp. 1–5.

[22] X. Yang, L. Ge, J. Wang, and C.-Y.-D. Sim, "A differentially driven dual-polarized high-gain stacked patch antenna," *IEEE Antennas Wireless Propag. Lett.*, vol. 17, no. 7, pp. 1181–1185, Jul. 2018.

[23] M. Barba, "A high-isolation, wideband and dual-linear polarization patch antenna," *IEEE Trans. Antennas Propag.*, vol. 56, no. 5, pp. 1472–1476, May 2008.

[24] A. Barka, A. Dorlé, and A. D. Oliveira Cabral, "Circularly polarized Ka-band radiating element unit-cell for SatCom wide-angle electronically steered phased arrays," in *Proc. IEEE Int. Symp. Antennas Propagat. USNC-URSI Radio Sci. Meet. (AP-S/URSI)*, 2022, pp. 139–140.

[25] A. Barka, A. D. O. Cabral Junior, A. Dorlé, B. Lesur, F. Peleau, and C. Melle, "Design, manufacturing and measurement of circularly polarized Ka-band radiating elements for SatCom wide-angle tile phased arrays," in *Proc. Int. Conf. Electrom. Adv. Appl. (ICEAA)*, 2023.

[26] R. B. Waterhouse, *Microstrip Patch Antennas: A Designer's Guide*, New York, NY, USA: Springer, 2003. [Online]. Available: https://link.springer.com/book/10.1007/978-1-4757-3791-2#bibliographic-information

[27] K. Statnikov, N. Sarmah, J. Grzyb, S. Malz, B. Heinemann, and U. R. Pfeiffer, "A 240 GHz circular polarized FMCW radar based on a SiGe transceiver with a lens-integrated on-chip antenna," in *Proc. 44th Eur. Microw. Conf.*, 2014, pp. 1750–1753.

[28] L. Zhang, Q. Zhang, and C. Hu, "The influence of dielectric constant on bandwidth of U-notch microstrip patch antenna," in *Proc. IEEE Int. Conf. Ultra-Wideband*, 2010, pp. 1–4.

[29] M. Kara, "Effects of substrate thickness on the properties of rectangular microstrip antenna elements," in *Proc. Asia-Pacific Microw. Conf. (AMPC)*, 1992, pp. 203–206.

[30] H. Kaouach, "Design and characterization of circularly polarized discrete lens antennas in 60-GHz band," *IEEE Antennas Wireless Propag. Lett.*, vol. 15, pp. 1200–1203, 2016.

[31] F. Wei, J.-W. Hao, L. Xu, and X. Shi, "A circularly polarized 3-D printed dielectric transmitarray antenna at millimeter-wave band," *IEEE Antennas Wireless Propag. Lett.*, vol. 20, pp. 1264–1268, 2021. [Online]. Available: https://ieeexplore.ieee.org/document/9423582/

[32] R. Madi, A. Clemente, and R. Sauleau, "A switchable linear to circular polarization converter using PIN diodes," in *Proc. Int. Symp. Antennas Propag. (ISAP)*, 2021, pp. 1–2.

[33] A. D. O. Cabral Junior, J. Pages-Mounic, A. Barka, and H. Kaouach, "Linearly polarized transmit-array operating in mmWave bands, design, optimization and demonstration," in *Proc. 16th Eur. Conf. Antennas Propagat. (EuCAP)*, 2022, pp. 1–5.

[34] F.-X. Roux and A. Barka, "Block Krylov recycling algorithms for FETI-2LM applied to 3-D electromagnetic wave scattering and radiation," *IEEE Trans. Antennas Propag.*, vol. 65, no. 4, pp. 1886–1895, Apr. 2017.

[35] J. Pages-Mounic, "Contribution to the design of compact X-band linear and circular polarization transmit-arrays," Ph.D. dissertation, Dept Eng. Phys., Universite De Toulouse, Dec. 2021. [Online]. Available: https://hal.science/tel-03552662

[36] H. Kaouach, L. Dussopt, J. Lanteri, T. Koleck, and R. Sauleau, "Wideband low-loss linear and circular polarization transmit-arrays in V-band," *IEEE Trans. Antennas Propag.*, vol. 59, no. 7, pp. 2513–2523, Jul. 2011.

[37] A. Gomez-Torrent et al., "A 38 dB gain, low-loss, flat array antenna for 320–400 GHz enabled by silicon-on-insulator micromachining," *IEEE Trans. Antennas Propag.*, vol. 68, no. 6, pp. 4450–4458, Jun. 2020.

[38] P.-Y. Feng, S.-W. Qu, and S. Yang, "Octave bandwidth transmitarrays with a flat gain," *IEEE Trans. Antennas Propag.*, vol. 66, no. 10, pp. 5231–5238, Oct. 2018. [Online]. Available: https://ieeexplore.ieee.org/document/8416719/